Published in final edited form as:
J Med Chem. 2010 October 28; 53(20): 7327–7336. doi:10.1021/jm100727t.

Targeted Mutations of *Bacillus anthracis* Dihydrofolate Reductase Condense Complex Structure-Activity Relationships

Jennifer M. Beierlein, **Nanda G. Karri**, and **Amy C. Anderson***
Dept. of Pharmaceutical Sciences, University of Connecticut, 69 N. Eagleville Rd., Storrs, CT 06269

Amy C. Anderson: Amy.Anderson@uconn.edu

Abstract

Several antifolates, including trimethoprim (TMP) and a series of propargyl-linked analogs, bind dihydrofolate reductase from *Bacillus anthracis* (BaDHFR) with lower affinity than is typical in other bacterial species. To guide lead optimization for BaDHFR, we explored a new approach to determine structure-activity relationships whereby the enzyme is altered and the analogs remain constant, essentially reversing the standard experimental design. Active site mutants of the enzyme, Ba(F96I)DHFR and Ba(Y102F)DHFR, were created and evaluated with enzyme inhibition assays and crystal structures. The affinities of the antifolates increase up to 60-fold with the Y102F mutant, suggesting that interactions with Tyr 102 are critical for affinity. Crystal structures of the enzymes bound to TMP and propargyl-linked inhibitors reveal the basis of TMP resistance and illuminate the influence of Tyr 102 on the lipophilic linker between the pyrimidine and aryl rings. Two new inhibitors test and validate these conclusions and show the value of the technique for providing new directions during lead optimization.

Keywords

Bacillus anthracis; dihydrofolate reductase; trimethoprim; antifolates; SAR

Introduction

In recent years, *Bacillus anthracis* dihydrofolate reductase (BaDHFR) has been investigated as a potential target in the treatment of the bacterial infection, anthrax[1]. Dihydrofolate reductase (DHFR), an essential enzyme in the folate biosynthetic pathway, has been pursued as a therapeutic target for several infectious diseases. DHFR is responsible for the reduction of dihydrofolate to tetrahydrofolate through a catalytic cycle involving nicotinamide adenine dinucleotide phosphate (NADPH) as a cofactor [2]. The DHFR active site is highly conserved across species, containing an acidic residue (typically Asp or Glu) at one end of a large hydrophobic pocket[3]. Potent antifolates contain a diaminopyrimidine or s-triazine pharmacophore that forms hydrogen bonds with the acidic residue and anchors the molecule in the pocket [3]. Key hydrophobic residues in the active site, including Leu 29, Val 32, Ile 51 and Phe 96 (Figure 1) form van der Waals interactions with the substrate and inhibitors.

*Corresponding author: Mailing address: Dept of Pharmaceutical Sciences, University of Connecticut, 69 N. Eagleville Rd., Storrs, CT 06269. Phone: (860)486-6145. Fax: (860)486-6857. amy.anderson@uconn.edu[1].

[1]Coordinates have been deposited in the Protein Data Bank with accession codes 3JVX, 3JWM, 3JWC, 3JWK, 3JWF, 3JW5, and 3JW3.

Supporting Information Available:
Table of measured IC_{50} values, non-linear regression plots for determination of enzyme kinetic parameters, omit density maps, NMR spectra and HPLC purity data are included.

BaDHFR, unlike DHFR from many bacteria, has been shown to be naturally insensitive to the broad spectrum antibiotic trimethoprim (TMP), which targets the DHFR enzyme. Studies have shown this lack of sensitivity to TMP results from low affinity for the enzyme[1c, 4]. We have previously described a series of DHFR inhibitors featuring a propargyl linker that shows an increased sensitivity to BaDHFR compared to TMP[1a]. The most potent inhibitor in this series shows a hundred-fold improvement over TMP. Crystal and solution structures of BaDHFR bound to this inhibitor have offered new insights into protein-ligand interactions critical to potency [1a, 5]. However, despite this improvement in potency over TMP, the propargyl-linked compounds generally exhibit affinities for BaDHFR that are ~100-fold less than other bacterial species such as *Staphylococcus aureus* [6].

The BaDHFR residues Phe 96 and Tyr 102, which are frequently isoleucine and phenylalanine in other TMP-sensitive bacterial species, may play an important role in the natural resistance of BaDHFR to TMP and the series of propargyl-linked analogs[1]. To further investigate the interactions of antifolates with these two residues, two mutant BaDHFR enzymes, Ba(F96I)DHFR and Ba(Y102F)DHFR were created by site-directed mutagenesis. Enzyme inhibition assays show that TMP and several of the propargyl-linked compounds have significantly greater affinity for the mutant Ba(Y102F)DHFR and approximately equal affinity for Ba(F96I)DHFR, suggesting that substitutions that interact with Tyr 102 are critical to determining potency. Structural analysis of seven wild type and mutant crystal structures bound to TMP and three propargyl-linked inhibitors reveal the basis of TMP resistance in the wild type enzyme and shed light on the influence of Tyr 102 on the lipophilic linker between the pyrimidine and aryl rings. The synthesis of two new propargyl-linked inhibitors validates these conclusions. Overall, these mutational studies aided in simplifying complex SAR data by revealing the critical impact of repulsive van der Waals' forces and electrostatics at key positions of the propargyl-linked antifolates.

Results

Previous structure-activity relationship (SAR) studies [1a, 5, 7] have generated almost fifty propargyl-linked analogs that have been evaluated with BaDHFR. Though increasingly potent inhibitors targeting BaDHFR have been designed [1a, 4], it has been difficult to obtain inhibitors with low nanomolar inhibition concentrations. Inhibition data indicates compound **9** (K_i = 0.33μM) is a viable lead compound[1a], however, modifications suggested by SAR and crystal structures have not improved its potency. For example, the crystal structure of compound **9** bound to BaDHFR[1a] (Figure 1) shows a large hydrophobic pocket enclosed primarily by Leu 55 and Leu 29, yet the addition of a second phenyl ring in place of the methoxy group (compound **11)** decreased potency (K_i = 1.65 μM).

Comparisons of sequence, structure and inhibition potency of selected analogs probed the differences between the active sites of BaDHFR and other bacterial species sensitive to TMP and the propargyl-linked analogs. BaDHFR and *Staphylococcus aureus* DHFR (SaDHFR) are 85% homologous (66% identical), yet there are striking differences between the two enzymes. Wild-type SaDHFR is sensitive to TMP, with a K_i of 0.0033 μM, while BaDHFR has a K_i of 24.1 μM. The series of propargyl-linked inhibitors have IC_{50} values as low as 5 nM [6a] in SaDHFR, yet the same compounds are consistently at least ten-fold less potent in BaDHFR. The most potent inhibitor for BaDHFR is compound **9**, with a K_i value of 300 nM, while in SaDHFR, the same compound has a K_i value of 9.9 nM [1a, 6a].

Resistance to TMP has developed in several bacterial species. In SaDHFR, a single mutation from Phe 98 to a tyrosine causes a 74-fold decrease in sensitivity [6a, 8]; recent studies indicate that this mutation may confer resistance by inducing an alternate conformation of the bound

cofactor, NADPH [6a]. In *Escherichia coli* DHFR (EcDHFR), and *Streptococcus pneumoniae* DHFR (SpDHFR), resistance has been observed when an isoleucine positioned near the methylene linker of TMP is mutated to a leucine [9]. A structural alignment (Figure 2) of BaDHFR to these other species reveals a tyrosine (Y102) in the same position where the mutation from a phenylalanine to tyrosine occurs in SaDHFR, and a phenylalanine (F96) in the same position as the isoleucine that mutates in EcDHFR and SpDHFR. To understand the effects of residues F96 and Y102 on the inhibition of TMP and the propargyl-linked analogs and to guide the optimal substitution of future analogs, mutant enzymes were prepared by site-directed mutation and evaluated with enzyme inhibition assays and structural studies.

Enzyme Activity

To begin, kinetic parameters for the enzymes were compared (Table 1). Interestingly, the Ba(Y102F)DHFR shows a slight improvement in K_M and only a two-fold loss in k_{cat}/K_M relative to the wild-type enzyme. The Ba(F96I)DHFR mutant, however, shows a much greater loss in K_M (~7-fold) and k_{cat}/K_M (~10-fold). This reduction is rationalized by the direct interaction of this residue with the substrate.

Enzyme Inhibition

K_i values for a representative sample of propargyl-linked inhibitors, reported in Table 2, were calculated using the Cheng-Prusoff method[10] from the experimental IC_{50} values obtained from competitive inhibition assayswith a substrate concentration of 100 μM and the experimental K_M values (experimental IC_{50} values are reported in Supporting Information). TMP was 50-fold more potent against Ba(Y102F)DHFR than the wild type enzyme. Interestingly, the Ba(F96I)DHFR mutation resulted in only a 2-fold improvement for TMP affinity. In fact, overall, the F96I mutation causes little to no difference in activity for the propargyl-linked compounds. Compound **9** stands out as the only ligand to lose significant activity against the Ba(F96I)DHFR mutant.

The mutation from a polar Tyr to a hydrophobic Phe at position 102 resulted in a four-fold improvement in binding for several of the propargyl-linked analogs, with some inhibitors, such as **1** and **3**, showing significantly greater (25- and 60-fold respectively) improvement. The Ba(Y102F)DHFR mutant enzyme appears to accommodate substituents on the propargyl linker more readily than the wild type enzyme. Compounds **1**, **3**, and **5** all show a ten-fold or greater improvement in enzyme inhibition as a result of this mutation. Compound **3** with a hydrophobic methyl substituent shows the greatest improvement, while compound **5** with a polar hydroxyl group shows the least improvement. The addition of a second phenyl ring, such as with compounds **14** and **15**, generally had little effect on activity against this mutant. The second phenyl ring is distant from the 102 residue, and is probably minimally affected by any steric or electrostatic effects caused by this mutation.

Structural Evaluation

For further evaluation of the effects of these mutations on the enzymes and their interactions with the ligands, the structures of BaDHFR bound to compounds **2** and **6**, Ba(F96I)DHFR bound to TMP, and Ba(Y102F)DHFR bound to compounds **2**, **5**, **6**, and TMP were determined by molecular replacement. All crystals belong to space group $P4_2$ and contain two monomers in the asymmetric unit. Relevant data collection and refinement statistics are reported for each crystal in Table 3. The structures show that both mutant enzymes conserve the canonical eight-stranded twisted β-sheet and four flanking α helices observed in the wild-type enzyme. Conserved hydrogen bonds between the side chain of Glu 28, an essential acidic residue, and the backbone carbonyl of Met 6 and Phe 96 (or Ile 96 in the F96I mutant)

with the pyrimidine ring of TMP and the propargyl-linked analogs are maintained in the mutant enzymes.

TMP Binding to Mutant BaDHFR Enzymes—Structures of TMP bound to both mutant DHFR enzymes reveal the factors involved in the natural resistance of the wild-type enzyme to TMP. Since TMP was bound to the protein by soaking rather than co-crystallization, TMP occupancy was verified by lower R_{free} and $R_{overall}$ values and a decrease in difference density relative to refinement with the original ligand. Omit maps (shown in Supporting Information) calculated for the two TMP structures according the method described by Bhat[11] also verify the presence of the TMP ligand. The two TMP-bound structures superimpose with an RMSD of 0.246 Å.

There is a dramatic change in active site volume caused by the F96I mutation, as shown by the electrochemical surfaces (Figure 3a). In order to best utilize the space gained by the presence of a smaller isoleucine rather than a bulky phenylalanine, there is a significant torsion angle difference between the pyrimidine and trimethoxyphenyl rings in the two mutants: the torsion angle, as defined by atoms C8, C9, C10 and C11 (Figure 3b), is 41.8° for TMP in Ba(F96I)DHFR and 24.0° for TMP in Ba(Y102F)DHFR. Energy calculations with Sybyl 8.1[12] using the Tripos force field and Gasteiger-Marsili charges show that the conformation of TMP adopted in the F96I mutant structure suffers an energy penalty of approximately 14 kCal/mol relative to the conformation observed in the Y102F mutant. This energy difference aids in explaining the 26-fold difference in K_i values for the two enzymes.

Inhibition data showing that the activity of TMP against Ba(Y102F)DHFR increases 50-fold compared to the wild-type enzyme indicates that Y102 may play a major role in the resistance of BaDHFR to TMP. Structural evidence suggests the change from a tyrosine to a phenylalanine increases the hydrophobicity of the pocket near the methylene linker of TMP, improving hydrophobic interactions (Figure 3). Crystal structures and enzyme inhibition data with Ba(Y102F)DHFR and propargyl-linked compounds further clarified the effects of this mutation in greater detail.

Analysis of Ba(Y102F)DHFR Structures—Structures with compounds **2**, **6** and **5**, possessing hydrogens, a methoxy group and a hydroxyl group, respectively, on the propargyl linker were determined to investigate the effect of the Y102F mutation (Figure 4). Racemic mixtures of compounds **5** and **6** were used in enzyme assays and protein crystallization. A clear preference for the *(S)* enantiomer of compound **6** and the (*R*) enantiomer of compound **5** appear in the electron density and yield lower R_{free} values in the refinement. The (*S)* enantiomer of compound **6** allows the methyl group of the methoxy substituent to interact with Leu 21 (not shown in Figure 4b for clarity) as well as to be oriented away from the polar pocket containing NADPH. The oxygen of the methoxy group is oriented to be within hydrogen bonding distance (2.80 Å) of Asn 47 (Figure 4B). The enzyme prefers the *(R)* enantiomer of **5** as the optimal configuration to form a hydrogen bond between the hydroxyl substituent and the side chain of Asn 47 (2.60 Å). The propargyl linker and trimethoxyphenyl ring of **5** are positioned closer to NADPH and the flanking helix than is observed with compound **6** (Figure 4C).

Clearly, the presence or absence of the hydroxyl group in BaDHFR (WT) or Ba(Y102F)DHFR, respectively, influences both the electrostatic and steric properties of the pocket. The RMSD between the structure of BaDHFR (WT) and the Y102F mutants bound to compounds **2** and **6** is only 0.17 Å, suggesting that the structure is only minimally perturbed by the removal of the hydroxyl group and that the influence of steric differences is limited. Furthermore, since the corresponding SaDHFR mutant (TMP resistant F98Y)

reflects a change in electrostatics, not in steric differences[6a], we investigated electrostatics in more depth.

Comparison of enzyme inhibition data within an analogous series of propargyl-linked compounds and energy calculations suggest that change in polarity from a tyrosine to a phenylalanine may have an advantageous effect on the lipophilic propargyl linker, particularly with a hydrophobic substituent. Comparing compounds **1**, **3** and **5**, which have a trimethoxyphenyl ring and various substituents on the propargyl linker, it is apparent that a propargylic hydrogen is preferred over a hydroxyl by 4-fold and by 8-fold over a methyl (H > OH > Me) with the wild-type enzyme. This trend is reversed for the Y102F mutant, with the propargylic hydrogen being preferred over a methyl by 4-fold and by 8-fold over a hydroxyl (H > Me > OH). Further supporting the fact that electrostatics most likely plays a role in determining activity, energy calculations performed with the structures of compound **6**, containing a methoxy propargylic substituent, and either F102 or Y102 (from the respective crystal structures) show that the former complex is 18.5 kcal/mol more favorable than the latter. In these calculations, the electrostatic energy changes by twice the extent that the van der Waals energy changes.

Understanding an outlier: Compound 9 Activity—Compound **9** suffers a 68-fold loss in affinity with the F96I mutation. It incurs the largest loss in potency of any propargyl-linked analog for either mutant enzyme. Previous structures of **9** bound to BaDHFR [1a, 5] placed the 2′ methoxy group near the NADPH cofactor, and the 5′ methoxy group facing towards Phe 96 (Figure 1 green conformation). The decrease in potency for other 2′,5′-substituted analogs (specifically such as compound **11**) confounded the apparent SAR and led to the theory that the aryl ring may be freely alternating between this conformation captured in the crystal structure and an inverted conformation that directs the 2′ methoxy group near Phe 96 and places the 5′ methoxy group near Asn 47, in a position analogous to the 3′ position of the trimethoxyphenyl ring of TMP (Figure 1 blue conformation). Mutation of Phe 96 to the smaller Ile reduces the van der Waals interactions that could favor this inverted conformation. The theory that compound **9** may be in two alternate conformations is supported by data from compound **8**, which has the same aryl ring as **9**. Compound **8** shows a 13-fold decrease in activity for the F96I mutant and is the only other compound to lose significant potency with the mutant enzyme. Inhibition data for compounds **11** and **10** also support the idea of a rotating phenyl ring. Compound **11** (K_i = 1.65 μM), with lower affinity than **9**, has a phenyl ring in place of the 5′ methoxy group of **9**, sterically restricting it from adopting the alternate conformation. Compound **10** (K_i = 0.41) lacks the 2′ methoxy group of **11**, yet exhibits increased affinity, showing that the 2′ methoxy group is not critical for binding. Examination of the electron density for the crystal of BaDHFR with compound **9** reveals that while the conformation with the 2′ methoxy group facing toward NADPH is preferred (as determined by minimal difference density), the alternate conformation is tolerated with some difference density present.

Synthesis and Evaluation of New Lead Compounds—To evaluate the ability of targeted site-directed mutagenesis to simplify complex SAR data and guide further analog design, two new propargyl-linked analogs were synthesized and tested against the wild-type and mutant BaDHFR enzymes. Both compounds incorporate a hydrogen at the propargyl position, as dictated by the Y102F mutant data. Additionally, compound **12** was synthesized to explore the effect of a bulky substitution at the 2′ position on the F96 residue, while compound **13** was synthesized to test the hypothesis that a 3′ methoxy group may be a more favorable substitution when compared to a 2′ methoxy group. Both compounds were accessed through a convergent route, employing a key Sonagashira coupling that has been used successfully to build the current library of propargyl-linked analogs[1a, 7], to join the

arene and pyrimidine fragments of the molecule. The two required propargylarenes were obtained through a series of reactions shown in Scheme 1. Phenol **18** was obtained in two steps from the commercially available 4-methoxyphenol[13]. Triflate addition to **18** afforded aryl triflate **19**. Suzuki cross-coupling to **19** gave the olefin **20** in excellent yield. Cleavage of **20** and subsequent reaction with the Ohira-Bestmann reaction gave alkyne **21**, which underwent Sonagashira coupling with 2,4-diamino-6-ethyl-5-iodo pyrimidine to give the final product **12**. Synthesis of **13** followed a similar route. Benzaldehyde **22** was obtained in two steps from commercially available 2,4-dibromoanisole [7b]. The Wittig reaction of **22** afforded the enol ether followed by direct hydrolysis to give the aldehyde **23**. Condensation of **22** with the Ohira-Bestmann reagent gave the terminal acetylene **24**. Sonagashira coupling afforded the final compound **13**.

Compounds **12** and **13** were tested against the wild-type and mutant enzymes (Table 2). As conclusions drawn from mutant data predicted, compound **12** lost activity with the increased steric bulk at the 2′ position, when compared to its two closest analogs, compounds **9** and **11,** due to its proximity to Phe 96. Validating the method of using targeted site directed mutations to aid ligand design, compound **13** proved to be the most potent biphenyl analog synthesized to date (K_i = 0.33μM), and further supported the hypothesis that a 3′ methoxy group is more favorable than a 2′ methoxy group since it is 4-fold more potent than the related 2′ analog, compound **11**. Inhibition data from compound **13** also supports the Y102F data by showing that an unsubstituted propargyl linker is preferable to a methyl substitution, since the potency of **13** improves on the activity of its methyl-substituted analog, compound **14**, by 8-fold.

Discussion

Site-directed mutagenesis has often been used to explore enzyme function, enzyme folding, and to assist with structural determination. Alanine scanning mutagenesis has been a particularly useful technique for studying the effects of specific amino acid side chains on protein function and binding [14]. While structural-activity relationship studies employing alanine scanning have largely focused on receptor interactions with small peptides [15], this technique has also been applied to investigate small molecule interactions [16]. To the best of our knowledge, however, rational site-directed mutagenesis has not been extensively applied to the interpretation of structure-activity relationships. These studies of mutant BaDHFR enzymes have shown a more directed approach to be a useful tool in understanding trends observed in the SAR data. For example, mutations in the BaDHFR active site revealed that the polar character of Y102 negatively impacts the enzyme's affinity with TMP and the propargyl-linked compounds, thus aiding in elucidating one factor of the enzyme's innate resistance to TMP. While polar propargylic substitutions may appear appealing, such substitutions have been shown in other species to have a negative impact on cell permeability[17]. Mutational studies also helped further interpret information gathered from structure-based drug design studies. Classical SAR suggested that a 2′ methoxy group was a beneficial substitution for the BaDHFR active site, however, traditional lead optimization has failed to improve on the activity of compound **9,** a relatively simple molecule. Now, with the data from the mutants, it is clear that the asymmetry of compound **9** and its ability to adopt alternate conformations enhances its entropic contribution to binding. Unfortunately, the ability of compound **9** to adopt these conformations is unique and viable lead optimization will most likely have to follow an independent path. The studies of mutant BaDHFR enzymes also helped further analyze the complex SAR data to understand the role of substituents on the propargyl linker of the lead compounds, as well as the effect of substitution patterns around the aryl ring. Currently, inhibitor development has been directed towards a methyl substituent on the propargyl bridge due to the efficacy seen in other DHFR species such as SaDHFR, *C. hominus* DHFR, and *C. glabrata* DHFR[6a, 7b, 17–18]. These

mutational studies indicate that a propargylic hydrogen would be a more favorable substituent for BaDHFR. This technique of targeted site-directed mutations derived from mutations observed in other species represents an interesting approach to reducing large amounts of complex SAR data for interpretation and can be used to better direct structure-based lead optimization.

Experimental

Enzyme cloning

Site-directed mutagenesis was used to change the earlier reported construct for BaDHFR-pET41[1a] to Ba(F96I)DHFR by a single point mutation. The Ba(F96I)-pET41 construct was amplified using PCR and inserted into vector pQE2 (Qiagen). Ba(F96I)-pQE2 clones were verified by sequencing. The resulting construct contained the Ba(F96I)DHFR gene with an N-terminal histidine and a DAPase stop point (Ile 2 was mutated to Arg) for future His-tag removal. Site-directed mutagenesis, amplification, and insertion in vector pQE2 was carried out in the same manner to change BaDHFR to Ba(Y102F)DHFR.

Recombinant Protein Expression and Purification

BaDHFR recombinant protein was expressed and purified according to reported procedures [1a]. Ba(F96I)DHFR recombinant protein was expressed in M15 cells upon induction with 1 mM IPTG at midlog phase. Protein expression was extended for an additional 6h at 37°C after induction. Cells were harvested by centrifugation. Pellets were lysed with 1x Bugbuster (Novagen) and DNase for 30 min at room temperature and then centrifuged at 4°C under high speed to collect the supernatant. The supernatant was loaded onto a nickel affinity column and was washed with 20 mM Tris, 1 mM DTT, 300 mM KCl (pH 8.0). Bound protein was eluted across a linear gradient with 20 mM Tris, pH 8.0, 1 mM DTT, 100 mM KCl, and 250 mM imidazole. Fractions with pure protein were concentrated to ~1 mL and loaded onto a size exclusion column (S200) for desalting. Protein was eluted into a final buffer of 20 mM Tris, 50 mM KCl, 5 mM DTT, and 0.5 mM EDTA. Fractions were analyzed by SDS-PAGE. Protein was concentrated to ~5 mg/mL, flash frozen, and stored at −80°C until use. Expression and purification of Ba(Y102F)DHFR was carried out in an identical manner.

Enzyme Assays

Enzyme activity assays were performed at 25°C by monitoring the rate of enzyme-dependent NADPH oxidation at an absorbance of 340 nm over several minutes [1a]. Reactions were performed in a buffer containing 20 mM TES, pH 7.0, 50 mM KCl, 10 mM 2-mercaptoethanol, 0.5 mM EDTA and 1 mg/mL BSA. All inhibition assays were performed with a single, limiting concentration of enzyme and saturating concentrations of NADPH and dihydrofolate (DHF). IC_{50} values were calculated as the average of three independent experiments. Standard reactions to determine the K_M of DHF were carried out using DHF concentrations of 25 μM, 50 μM, 100 μM, 150 μM, and 200 μM. Activity at each concentration was calculated as the average of three independent experiments. All supporting data for enzyme activity is reported in Supplementary Information.

Crystallization

Protein (5 mg/mL) was incubated with 2 mM NADPH and 2 mM ligand for 1 h at 4°C. After incubation, the protein-ligand complex was concentrated to ~15 mg/mL using a microcon (Amicon). Initial crystal hits were grown at room temperature by hanging drop diffusion in 22.5% (w/v) PEG 10,000, 0.1 M MES, pH 6.75, at an equal ratio of protein to crystallization solution. Microseeding was used to obtain isolated crystals in 12% (w/v) PEG 10,000 and 0.1 MES, pH 6.75 at a protein concentration of 12 mg/mL. TMP-bound protein

crystals were obtained by soaking good quality crystals, co-crystallized with compound **6**, with 10 mM TMP in DMSO at room temperature for two days. Crystals were cryoprotected in 15% ethylene glycol and flash frozen with liquid nitrogen. Data were collected at Brookhaven National Synchrotron Light Source on beamlines X29A and X25. All data sets were collected at 100 K.

Structure Determination

All structures were solved by molecular replacement. The program Phaser [19] and a model of BaDHFR (PDB code 3E0B[1a]) were used to determine initial phase information. The program Coot [20] was used to visualize the electron density map and build the model. The model was refined with the program Refmac5[21]. Models were validated using Ramachandran plots and Procheck [22].

Synthesis

The ^{1}H and ^{13}C NMR spectra were recorded on Bruker instruments at 500 and 125 MHz. Chemical shifts are reported in ppm and are referenced to residual $CHCl_3$ solvent; 7.26 and 77.0 ppm for ^{1}H and ^{13}C respectively. Melting points were recorded on Mel-Temp 3.0 apparatus and are uncorrected. High-resolution mass spectroscopy was provided by the *Notre Dame Mass Spectrometry Laboratory.* TLC analyses were performed on Whatman Partisil K6F silica gel 60 plates. All glassware was oven-dried and allowed to cool under an argon atmosphere. Anhydrous dichloromethane, ether, and tetrahydrofuran were used directly from Baker cycletainers. Anhydrous dimethylformamide was purchased from Acros and degassed by purging with argon. Anhydrous triethylamine was purchased from Aldrich and degassed by purging with argon. All reagents were used directly from commercial sources unless otherwise stated. 2-Allyl-4-methoxyphenol was synthesized according to literature procedures[13]. 3-methoxy-5-phenylbenzaldehyde was synthesized according to literature procedures[7b]. The Ohira-Bestmann reagent was synthesized according to literature procedures [23]. 2,4-Diamino-5-iodo-6-ethylpyrimidine was synthesized according to literature procedures [7a]. Both final compounds had a purity of >95% as determined by HPLC analysis in two mobile phase conditions (Please see Supporting Information for more details).

2-allyl-4-methoxyphenyl trifluoromethanesulfonate (19)—To a round-bottom flask under argon, 2-allyl-4-methoxyphenol **17** (2.00g, 12.2 mmol) and pyridine (2.93 mL, 36.6 mmol) was dissolved in 67 mL dichloromethane. A solution of trifluoroacetic acid (2.25 mL, 13.4 mmol) in 34 mL of dichloromethane was added dropwise over several minutes. The reaction mixture was then stirred at room temperature for 1 h. After completion, the reaction was quenched with 67 mL H_2O and the layers were separated. The aqueous layer was extracted with dichloromethane (48 mL, 3x). The combined organics were washed with H_2O (60 mL),10% HCl (60 mL) and brine (60 mL), dried over anhydrous Na_2SO_4, and concentrated to afford **19** as a red oil (3.33g, 92%). The product was taken onto the next step without further purification: TLC R_f = 0.76 (9:1 Hex:EtOAc); ^{1}H NMR ($CDCl_3$) δ 7.20 (d, *J* =3.3,1 H), 6.5 (d, J = 6.7, 1H), 6.82-6.80 (dq, *J* = 6.7, 1 H), 5.97-5.91 (m, 1H), 5.21-5.16 (m, 2H), 3.83 (s, 3H), 3.48 (d, *J*=5.0, 2H); ^{13}C NMR ($CDCl_3$) δ 159.0, 141.4, 134.3, 122.3, 119.9, 117.6, 117.4, 116.2, 114.8, 112.8, 55.6, 34.2; HRMS (FAB, M^+) *m/z* 297.0403 (calculated for $C_{11}H_{11}F_3O_4S$, 297.0364).

2-allyl-4methoxybiphenyl (20)—To an oven-dried sealed tube was added triflate **19** (1.50 g, 5.0 mmol), phenylboronic acid (778.5 mg, 5.6 mmol), $Pd(P(Ph)_3)_4$ (151.8 mg, 0.13 mmol), K_3PO_4 (1.61 g, 7.6 mmol), and anhydrous dioxane (25.2 mL). The mixture was stirred and then degassed once using the freeze/pump/thaw method. Once the mixture warmed to room temperature, the vessel was sealed under argon and placed in an 85°C oil

bath for 48 h. The dark colored mixture was cooled, diluted with ether (10 mL), and filtered through a pad of silica gel (~20 g), rinsing with ether. The filtrate was concentrated and the residue purified by flash chromatography (SiO_2, 94 g, 1% EtOAc/hexanes) to afford the olefin **20** as a colorless oil (1.13g, 99%): TLC R_f = 0.68 (9:1 Hex: EtOAc); ^{1}H NMR ($CDCl_3$) δ 7.49 (t, *J* = 5.9, 2 H), 7.43 (t, *J* = 5.9, 3H), 7.31 (d, *J* = 5.9, 1H), 6.98 (d, *J* =20.5, 1H), 6.94 (dd, *J* = 20.5, 1H), 6.01 (m, 1H), 5.16 (dd, *J* = 20.5, 1H), 5.10 (dd, *J* =20.5, 1H), 3.90 (s, 1H), 3.45 (d, *J* = 6.83, 2H); ^{13}C NMR ($CDCl_3$) δ 159.1, 141.5, 138.7, 137.6, 134.7, 131.2, 129.6, 128.1, 126.7, 116.0, 115.2, 111.6, 55.3, 37.8; HRMS (FAB, M^+) *m/z* 225.1274 (calculated for $C_{16}H_{16}O$, 225.1235).

4-methoxy-2-(prop-2-ynyl)biphenyl (21)—To a round bottom flask, olefin **20** (0.678 g, 3.0 mmol), OsO_4 (21.6 mg, 0.058 mmol), and $NaIO_4$ (2.55 g, 11.9 mmol) were suspended in dioxane (22 mL), and H_2O (7.4 mL). The reaction mixture was stirred for 1 h at room temperature. After 1 h, the reaction mixture was diluted with H_2O (35 mL) and Et_2O (90 mL) and the layers were separated. The aqueous layer was extracted with Et_2O (45 mL, 3x). The combined organics were washed with brine (90 mL), dried over anhydrous Na_2SO_4, and concentrated to afford the crude aldehyde.

To a 0°C solution of the crude aldehyde in MeOH (3.9 mL) was added the Ohira-Bestmann reagent (1.70 g, 9.0 mmol) dissolved in MeOH (6.6 mL) followed by powdered, anhydrous K_2CO_3(0.705 g, 5.11 mmol). The mixture was stirred at 0°C for 2 h. After 2 h, MeOH was removed under vacuum. The residue was dissolved in water and ether (50 mL each). The organic phase was separated and the aqueous phase extracted with additional ether (3 × 50 mL). The combined extracts were washed with saturated $NaHCO_3$ (50 mL) and brine (50 mL), dried over Na_2SO_4, and concentrated to afford the crude product that was purified by flash chromatography (SiO_2, 75 g, 1% EtOAc/Hexanes) to afford alkyne **21** as a colorless oil (0.2009 g, 38%): TLC R_f = 0.69 (9:1 Hex: EtOAc); ^{1}H NMR ($CDCl_3$) δ 7.50 (m, 2 H), 7.44 (m, 3H), 7.35 (s, 1H), 7.28 (m, 1H), 6.97 (m, 1H), 3.94 (s, 3H), 3.61 (s, 2H), 2.27 (s, 1H); ^{13}C NMR ($CDCl_3$) δ 159.3, 140.8, 135.1, 134.1, 131.2, 129.4, 128.4, 128.1, 127.0, 114.5, 112.5, 82.6, 55.4, 23.4; HRMS (FAB, M^+) *m/z* 223.1105 (calculated for $C_{16}H_{15}O$, 223.1117).

2,4-Diamino-5-[3-(2-phenyl-5-methoxyphenyl)prop-1-ynyl]-6-ethylpyrimidine (12)—To an oven-dried sealed tube was added 2,4-diamino-6-ethyl-5-iodopyrimidine (97.8 mg, 0.37 mmol), $Pd(PPh_3)_2Cl_2$ (29.3 mg, 0.037 mmol), CuI (15.0 mg, 0.080 mmol) and acetylene **21** (189.2 mg, 0.74 mmol). Degassed (argon purge) anhydrous DMF and triethylamine (0.53 mL each) were added, the tube was sealed and the mixture degassed by one cycle of freeze-pump-thaw. The mixture was stirred at 60°C for 18 h and then added to a separatory funnel containg EtOAc (16 mL). The organic layer was washed twice with a water/saturated $NaHCO_3$ solution (1:2, 16 mL) and then brine (16 mL). The organic layer was then dried over Na_2SO_4 and concentrated under reduced pressure. The residue was purified by flash chromatography (SiO_2, 100 g, EtOAc) to afford the coupled product **12** as a white powder (68.7 mg, 51.4%). An analytical sample was obtained by crystallization from EtOAc. TLC R_f = 0.29 (EtOAc); m.p. = 195.2-196.6°C; ^{1}H NMR ($CDCl_3$) δ 7.46 (t, *J* = 6.3, 2 H), 7.38 (t, *J* = 6.25, 3H), 7.22 (m, 2H), 6.90 (dd, *J* =5.0, 1H), 3.89 (s, 3H), 3.81 (s, 2H), 2.68 (q, *J* = 5.0, 2H), 1.24 (t, *J* = 5.0, 3H) ; ^{13}C NMR ($CDCl_3$) δ 164.3, 160.6, 159.2, 140.8, 135.7, 134.0, 131.2, 129.4, 128.4, 128.0, 127.0, 114.3, 112.3, 96.9, 90.7,75.5, 55.4, 29.7, 24.9, 12.6; HRMS (FAB M^+) *m/z* 359.1857 (calculated for $C_{22}H_{23}N_4O$, 359.1866) ; HPLC (a) t_R= 11.32 min, 96.8%, (b) t_R= 33.62, 96.9%

2-(5-methoxybiphenyl-3-yl)acetaldehyde (23)—To a 0°C suspension of methoxymethyltriphenylphosphonium chloride (3.50g, 10.2 mmol) in dry THF (30.5 mL)

under an argon atmosphere was added NaO^{t}Bu (1.45g, 15.1 mmol) in one portion. The red-orange suspension was stirred for a further 0.5 h at 0°C. Then a solution of 3-methoxy-5-phenylbenzaldehyde **22** (1.23g, 5.8 mmol) in THF (10.0 mL) was added dropwise. Following 20 min., the reaction was quenched with water (97.5 mL) and diluted with ether (60 mL). The organic phase was separated and the aqueous phase extracted with additional ether (3 × 97.5 mL). The combined extracts were washed with brine (60 mL), dried over Na_2SO_4, and concentrated to afford the crude product that was filtered through a column of silica (90 g, 2–5% EtOAc/Hexanes) to afford 1.31g of a mixture of enol ethers (*E/Z* ≈ 60:40) that were immediately hydrolyzed in the subsequent step.

To a solution of enol ether (1.31 g, 5.44 mmol) in THF (34 mL) was added concentrated HCl (2.3 mL). The solution was warmed to 55°C and stirred for 1 h. After 1 h, TLC showed the starting material had been consumed. The mixture was cooled and diluted with water and ether (88 mL each). The organic phase was separated and the aqueous phase extracted with additional ether (2 × 88 mL). The combined extracts were washed with saturated $NaHCO_3$ (88 mL) and brine (88 mL), dried over Na_2SO_4, and concentrated to afford the crude product that was purified by flash chromatography (SiO_2, 140 g, 5% EtOAc/Hexanes) to afford aldehyde **23** as a colorless oil (0.3343 g, 26.8%): TLC R_f = 0.13 (9:1 Hex: EtOAc); ^{1}H NMR ($CDCl_3$) δ 9.81 (s, 1H), 7.63 (d, *J* = 7.6, 2H), 7.49 (t, *J*= 7.6, 2H), 7.41 (t, *J* =7.6, 1H), 7.12 (s, 1H), 7.08 (s, 1H), 6.80 (s, 1H), 3.90 (s, 3H), 3.74 (s, 2H); ^{13}C NMR ($CDCl_3$) δ 199.2, 160.5, 143.5, 140.7, 133.7, 128.9, 127.7, 127.3, 121.0, 114.1, 111.9, 55.5, 50.7; HRMS (FAB, M^+) *m/z* 227.1062 (calculated for $C_{15}H_{15}O_2$, 227.1067).

3-methoxy-5-(prop-2-ynyl)biphenyl (24)—To a 0°C solution of aldehyde **23** (0.334 g, 1.46 mmol) in MeOH (2.0 mL) was added the Ohira-Bestmann reagent (0.831 g, 4.38 mmol) dissolve in MeOH (3.0 mL) followed by powdered, anhydrous K_2CO_3(0.340 g, 2.46 mmol). The mixture was stirred at 0°C for 2 h. After 2 h, removed MeOH under vacuum. Residue was dissolved in water and ether (23 mL each). The organic phase was separated and the aqueous phase extracted with additional ether (3 × 23 mL). The combined extracts were washed with saturated $NaHCO_3$ (23 mL) and brine (23 mL), dried over Na_2SO_4, and concentrated to afford the crude product that was purified by flash chromatography (SiO_2, 30 g, 1% EtOAc/Hexanes) to afford alkyne **24** as a colorless oil (0.1987 g, 61.2%): TLC R_f = 0.42 (9:1 Hex: EtOAc); ^{1}H NMR ($CDCl_3$) δ 7.71(d, *J* = 8.0, 2H), 7.55 (t, *J*= 8.0, 2H), 7.48 (t, *J* =8.0, 1H), 7.30 (s, 1H), 7.15 (s, 1H), 7.05 (s, 1H), 3.95 (s, 3H), 3.75 (s, 2H), 2.36 (s, 1H); ^{13}C NMR ($CDCl_3$) δ 160.3, 143.0, 141.1, 138.1, 128.9, 127.7, 127.3, 119.5, 112.5,111.4, 81.9, 71.0, 55.4, 25.0; HRMS (FAB, M^+) *m/z* 223.1115 (calculated for $C_{16}H_{15}O$, 223.1117).

2,4-Diamino-5-[3-(2-methoxy-5-phenylphenyl)prop-1-ynyl]-6-ethylpyrimidine (13)—To an oven-dried sealed tube was added 2,4-diamino-6-ethyl-5-iodopyrimidine (117.9 mg, 0.45 mmol), $Pd(PPh_3)_2Cl_2$ (31.6 mg, 0.045 mmol), CuI (8.5 mg, 0.045 mmol) and acetylene **24** (198.7 mg, 0.89 mmol). Degassed (argon purge) anhydrous DMF and triethylamine (2.25 mL each) were added, and the tube was sealed and the mixture degassed by one cycle of freeze-pump-thaw. The mixture was stirred at 60°C for 18 h and then added to a separatory funnel containg EtOAc (17 mL). The organic layer was washed twice with a water/saturated $NaHCO_3$ solution (1:2, 7 mL) and then brine (7 mL). The organic layer was then dried over Na_2SO_4 and concentrated under reduced pressure. The residue was purified by flash chromatography (SiO_2, 15 g, EtOAc) to afford the coupled product **13** as a light yellow powder (103.9 mg, 64.4%). An analytical sample was obtained by dissolving in chloroform and precipitation with hexane. TLC R_f = 0.23 (EtOAc); m.p. = 156.7–158.5°C; ^{1}H NMR ($CDCl_3$) δ 7.61 (d, *J* =6.6, 2 H), 7.47 (t, *J* = 6.6, 2H), 7.38 (t, *J* =6.6, 1H), 7.24(s, 1H),7.05 (s, 1H), 6.98(s, 1H), 5.22(s, 2H), 4.95(s, 2H), 3.96 (s, 2H), 3.90 (s, 3H),

2.75 (q, *J*=6.4, 2H), 1.26 (t, *J*=, 3H) ; ^{13}C NMR ($CDCl_3$) 173.4, 164.5, 160.8, 160.3, 143.0, 140.9, 138.8, 128.8, 127.6, 127.1, 119.3, 112.4, 111.2, 96.2, 90.5, 75.8, 55.4, 29.6, 26.4, 12.7; HRMS (FAB, M^+) *m/z* 359.1858 (calculated for $C_{22}H_{23}N_4O$, 359.1856) ; HPLC (a) t_R= 11.28 min, 98.2%, (b) t_R= 33.14, 98.2%.

Supplementary Material

Refer to Web version on PubMed Central for supplementary material.

Acknowledgments

The authors gratefully acknowledge Janet Paulsen for assisting with energy calculations and the support of the NIH AI073375.

Abbreviations

DHFR	dihydrofolate reductase
BaDHFR	dihydrofolate reductase from *Bacillus anthracis*
TMP	trimethoprim
DHF	dihydrofolate
SaDHFR	dihydrofolate reductase from *Staphylococcus aureus*
EcDHFR	dihydrofolate reductase from *Escherichia coli*
SpDHFR	dihydrofolate reductase from *Streptococcus pneumoniae*
hDHFR	human dihydrofolate reductase
NADPH	nicotinamide adenine dinucleotide phosphate, reduced form

References

1. (a) Beierlein JM, Frey KM, Bolstad DB, Pelphrey PM, Joska TM, Smith AE, Priestley ND, Wright DL, Anderson AC. Synthetic and Crystallographic Studies of a New Inhibitor Series Targeting *Bacillus anthracis* Dihydrofolate Reductase. Journal of Medicinal Chemistry. 2008; 51(23):7532–7540. [PubMed: 19007108] (b) Bennett BC, Xu H, Simmerman RF, Lee RE, Dealwis CG. Crystal Structure of the Anthrax Drug Target, Bacillus anthracis Dihydrofolate Reductase†. Journal of Medicinal Chemistry. 2007; 50(18):4374–4381. [PubMed: 17696333] (c) Barrow EW, Bourne PC, Barrow WW. Functional Cloning of Bacillus anthracis Dihydrofolate Reductase and Confirmation of Natural Resistance to Trimethoprim. Antimicrob Agents Chemother. 2004; 48(12):4643–4649. [PubMed: 15561838]
2. Anderson AC. Targeting DHFR in parasitic protozoa. Drug Discovery Today. 2005; 10(2):121–128. [PubMed: 15718161]
3. Cody V, Schwalbe CH. Structural characteristics of antifolate dihydrofolate reductase enzyme interactions. Crystallography Reviews. 2006; 12(4):301–333.
4. Barrow EW, Dreier J, Reinelt S, Bourne PC, Barrow WW. In Vitro Efficacy of New Antifolates against Trimethoprim-Resistant *Bacillus anthracis*. Antimicrob Agents Chemother. 2007; 51(12): 4447–4452. [PubMed: 17875993]
5. Beierlein JM, Deshmukh L, Frey KM, Vinogradova O, Anderson AC. The Solution Structure of *Bacillus anthracis* Dihydrofolate Reductase Yields Insight into the Analysis of Structure Activity Relationships for Novel Inhibitors. Biochemistry. 2009; 48(19):4100–4108. [PubMed: 19323450]
6. (a) Frey KM, Liu J, Lombardo MN, Bolstad DB, Wright DL, Anderson AC. Crystal Structures of Wild-type and Mutant Methicillin-resistant *Staphylococcus aureus* Dihydrofolate Reductase Reveal an Alternate Conformation of NADPH That May Be Linked to Trimethoprim Resistance. Journal of Molecular Biology. 2009; 387(5):1298–1308. [PubMed: 19249312] (b) Frey KM, Lombardo MN,

Wright DL, Anderson AC. Towards the understanding of resistance mechanisms in clinically isolated trimethoprim-resistant, methicillin-resistant Staphylococcus aureus dihydrofolate reductase. Journal of Structural Biology. 2010; 170(1):93–97. [PubMed: 20026215]

7. (a) Pelphrey PM, Popov VM, Joska TM, Beierlein JM, Bolstad ESD, Fillingham YA, Wright DL, Anderson AC. Highly Efficient Ligands for Dihydrofolate Reductase from *Cryptosporidium hominis* and *Toxoplasma gondii* Inspired by Structural Analysis. Journal of Medicinal Chemistry. 2007; 50(5):940–950. [PubMed: 17269758] (b) Bolstad DB, Bolstad ESD, Frey KM, Wright DL, Anderson AC. Structure-Based Approach to the Development of Potent and Selective Inhibitors of Dihydrofolate Reductase from Cryptosporidium. Journal of Medicinal Chemistry. 2008; 51(21): 6839–6852. [PubMed: 18834108]
8. (a) Dale G, Broger C, Hartman P, Langen H, Page M, Then R, Stuber D. Characterization of the gene for the chromosomal dihydrofolate reductase (DHFR) of *Staphylococcus epidermidis* ATCC 14990: the origin of the trimethoprim-resistant S1 DHFR from *Staphylococcus aureus*? J Bacteriol. 1995; 177(11):2965–2970. [PubMed: 7768789] (b) Dale GE, Broger C, D'Arcy A, Hartman PG, DeHoogt R, Jolidon S, Kompis I, Labhardt AM, Langen H, Locher H, Page MGP, Stüber D, Then RL, Wipf B, Oefner C. A single amino acid substitution in Staphylococcus aureus dihydrofolate reductase determines trimethoprim resistance. Journal of Molecular Biology. 1997; 266(1):23–30. [PubMed: 9054967]
9. (a) Maskell JP, Sefton AM, Hall LMC. Multiple Mutations Modulate the Function of Dihydrofolate Reductase in Trimethoprim-Resistant *Streptococcus pneumoniae*. Antimicrob Agents Chemother. 2001; 45(4):1104–1108. [PubMed: 11257022] (b) Watson M, Jian-Wei L, Ollis D. Directed evolution of trimethoprim resistance in Escherichia coli. FEBS Journal. 2007; 274(10):2661–2671. [PubMed: 17451440]
10. Cheng YC, Prusoff WH. Relationship between the inhibition constant (KI) and the concentration of inhibitor which causes 50 per cent inhibition (I50) of an enzymatic reaction. Biochemical Pharmacology. 1973; 22(23):3099–3108. [PubMed: 4202581]
11. Bhat TN, Cohen GH. OMITMAP: An electron density map suitable for the examination of errors in a macromolecular model. Journal of Applied Crystallography. 1984; 17(4):244–248.
12. SYBYL 7.3. Tripos International; 1699 South Hanley Rd. St. Louis, Missouri, 63144, USA:
13. Brimble MA, Flowers CL, Trzoss M, Tsang KY. A facile synthesis of fused aromatic spiroacetals based on the 3,4,3′,4′-tetrahydro-2,2′-spirobis(2H-1-benzopyran) skeleton. Tetrahedron. 2006; 62(25):5883–5896.
14. (a) Sidhu SS, Kossiakoff AA. Exploring and designing protein function with restricted diversity. Current Opinion in Chemical Biology. 2007; 11(3):347–354. [PubMed: 17500026] (b) Weir, MPM. Fiona Hamilton Methods for production of conformationally stable G protein-coupled receptor mutants for use in drug screening ligands. WO 2009081136. 2009. p. A2(c) DeLano WL. Unraveling hot spots in binding interfaces: progress and challenges. Current Opinion in Structural Biology. 2002; 12(1):14–20. [PubMed: 11839484] (d) Morrison KL, Weiss GA. Combinatorial alanine-scanning. Current Opinion in Chemical Biology. 2001; 5(3):302–307. [PubMed: 11479122]
15. (a) Gkountelias K, Tselios T, Venihaki M, Deraos G, Lazaridis I, Rassouli O, Gravanis A, Liapakis G. Alanine Scanning Mutagenesis of the Second Extracellular Loop of Type 1 Corticotropin-Releasing Factor Receptor Revealed Residues Critical for Peptide Binding. Molecular Pharmacology. 2009; 75(4):793–800. [PubMed: 19124613] (b) Ueda S, Oishi S, Wang Z-x, Araki T, Tamamura H, Cluzeau J, Ohno H, Kusano S, Nakashima H, Trent JO, Peiper SC, Fujii N. Structure Activity Relationships of Cyclic Peptide-Based Chemokine Receptor CXCR4 Antagonists: Disclosing the Importance of Side-Chain and Backbone Functionalities. Journal of Medicinal Chemistry. 2006; 50(2):192–198. [PubMed: 17228861] (c) Gauguin L, Delaine C, Alvino CL, McNeil KA, Wallace JC, Forbes BE, De Meyts P. Alanine Scanning of a Putative Receptor Binding Surface of Insulin-like Growth Factor-I. Journal of Biological Chemistry. 2008; 283(30):20821–20829. [PubMed: 18502759] (d) Cotter PD, Deegan LH, Lawton EM, Draper LA, O'Connor PM, Hill C, Ross RP. Complete alanine scanning of the two-component lantibiotic lacticin 3147: generating a blueprint for rational drug design. Molecular Microbiology 2006. 62(3):735–747.

16. Yamada S, Yamamoto K. Ligand Recognition by Vitamin D Receptor: Total Alanine Scanning Mutational Analysis of the Residues Lining the Ligand Binding Pocket of Vitamin D Receptor. Current Topics in Medicinal Chemistry. 2006; 6(12):1255–1265. [PubMed: 16848739]

17. Liu J, Bolstad DB, Bolstad ESD, Wright DL, Anderson AC. Towards New Antifolates Targeting Eukaryotic Opportunistic Infections. Eukaryotic Cell. 2009; 8(4):483–486. [PubMed: 19168759]

18. Frey KM, Lombardo MN, Wright DL, Anderson AC. Towards the understanding of resistance mechanisms in clinically isolated trimethoprim-resistant, methicillin-resistant *Staphylococcus aureus* dihydrofolate reductase. Journal of Structural Biology. 2010; 170:93–97. [PubMed: 20026215]

19. McCoy AJ. Solving structures of protein complexes by molecular replacement with Phaser. Acta Crystallographica Section D, Biological crystallography. 2007; 63(1):32–41.

20. Emsley P, Cowtan K. Coot: model-building tools for molecular graphics. Acta Crystallographica: Section D. 2004; 60(12p1):2126–2132.

21. Murshudov GNVAA, Dodson EJ. Refinement of macromolecular structures by the maximum-likelihood method. Acta Crystallographica Section D, Biological crystallography. 1997; 53(3): 240–255.

22. Laskowski RAM, Malcolm W, Moss David S, Thornton Janet M. PROCHECK: a program to check the stereochemical quality of protein structures. Journal of Applied Crystallography. 1993; 26(2):283–291.

23. Pietruszka J, Witt A. Synthesis of the Bestmann-Ohira Reagent. Synthesis. 2006; 2006(24):4266–4268.

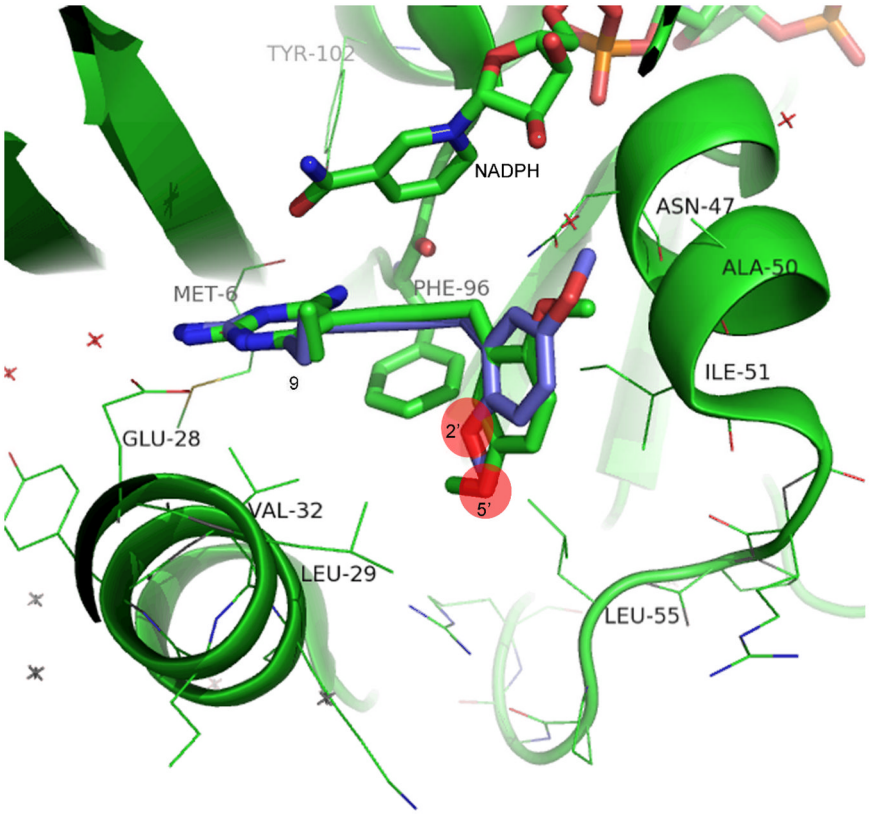

Figure 1.

Compound **9** bound to BaDHFR (WT). The original conformation of **9** from PDB ID 30B is shown in green; the alternate conformation stabilized by F96I is shown in blue. The two red circles indicate the positions of the 2′ and 5′methoxy groups in the two alternate conformations. (*Figure prepared in PyMol).*

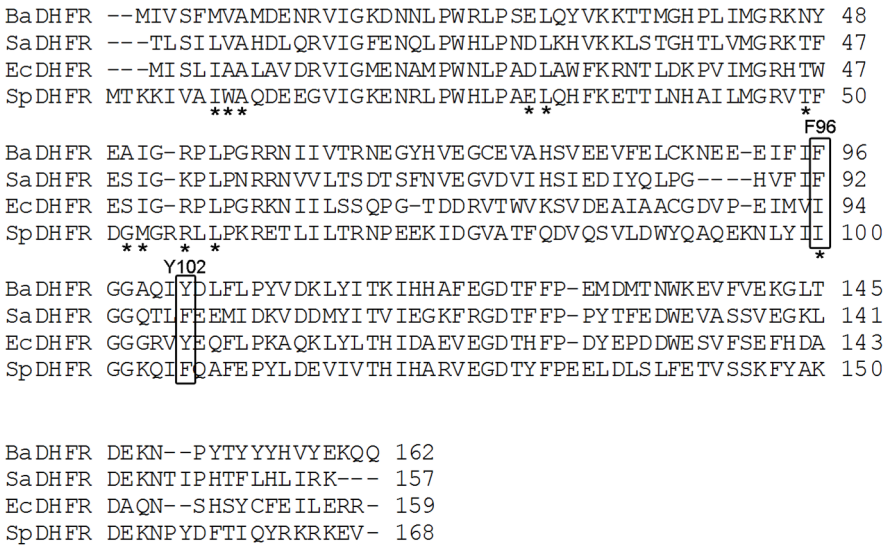

Figure 2.
Structural Alignment of BaDHFR, SaDHFR, EcDHFR, and SpDHFR.
* indicates active site residues.

TMP Binding to Mutant BaDHFR Enzymes

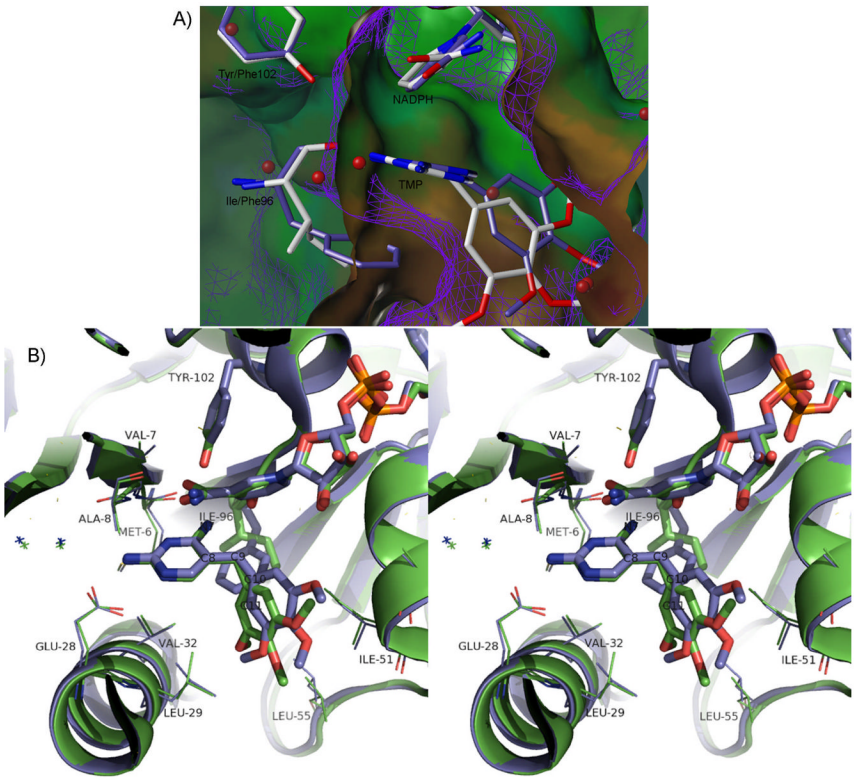

Figure 3.

A) Lipophilic potential surface diagrams of Ba(F96I)DHFR (white sticks and solid surface) and Ba(Y102F)DHFR (purple sticks and mesh surface). (Created using Sybyl 8.0) B) Active site stereo view of TMP bound to Ba(F96I)DHFR (green) and to Ba(Y102F)DHFR (blue). (Created using PyMol)

Analysis of Ba(Y102F)DHFR Structures

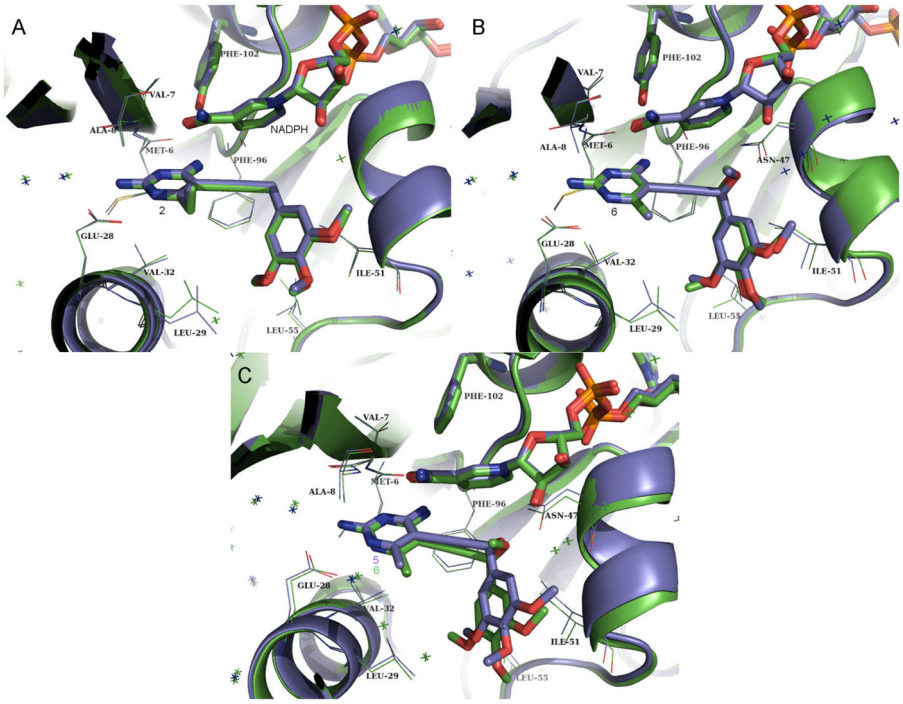

Figure 4.

A) Compound **2** bound to BaDHFR (green) and to Ba(Y102F)DHFR (blue). B) Compound **6** bound to BaDHFR (green) and to Ba(Y102F)DHFR (blue). C) Compound **6** bound to Ba(Y102F)DHFR (green) and compound **5** bound to Ba(Y102F)DHFR (blue). Figures generated using PyMol.

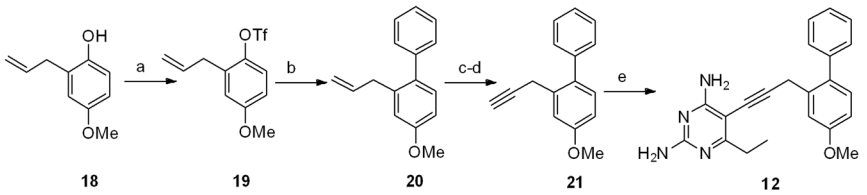

18 19 20 21 12

[a] a) Trifluoroacetic acid, pyridine, DCM, RT, 1h, 92%; b) $PhB(OH)_2$, $Pd(P(Ph)_3)_4$, K_3PO_4, Dioxane, 85°C, 48h, 99%; c)OsO_4, $NaIO_4$, Dioxane, H_2O, RT, 1h; d) dimethyl (1-diazo-2-oxopropyl)phosphonate, K_2CO_3, MeOH, 0°C, 2 h, 38%; (2 steps); e) 2,4-diamino-6-ethyl-5-iodopyrimidine, $Pd(P(Ph)_3)_2Cl_2$, CuI, DMF, Triethylamine, 60°C, 18h, 51.4%.

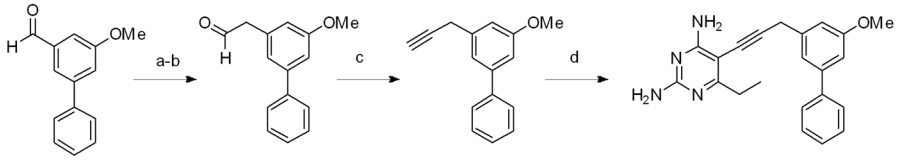

22 23 24 13

[b] a) PH_3PCH_2OMeCl, NaO^tBu, THF, 0°C; b) concentrated HCl, THF, reflux, 1h, 26.8% (2 steps); c) dimethyl (1-diazo-2-oxopropyl)phosphonate, K_2CO_3, MeOH, 0°C, 2 h,61%; d) 2,4-diamino-6-ethyl-5-iodopyrimidine, $Pd(P(Ph)_3)_2Cl_2$, CuI, DMF, Triethylamine, 60°C, 64%.

Scheme 1.
Synthesis of Compounds **12**[a] and **13**[b].

Table 1

K_M and k_{cat} values for wild type and mutant enzymes

	K_M (μM)	k_{cat} (sec^{-1})	k_{cat}/K_M
BaDHFR	33.7 ± 3.2	9.3	0.28
Ba(F96I)DHFR	230.1 ± 33.97	4.8	0.02
Ba(Y102F)DHFR	14.44 ± 1.736	1.7	0.12

Table 2

K_i Values of Inhibitors against Wild Type and Mutant Enzymes

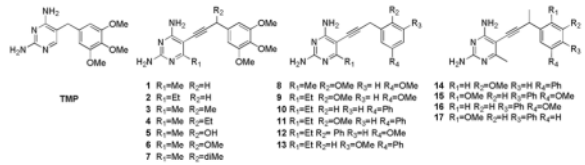

Ligand	BaDHFR K_i (μM)	BaF96IDHFR K_i (μM)	Fold Difference	BaY102FDHFR K_i (μM)	Fold Difference
TMP	24.1 ± 0.03	13.7 ± 0.51	1.8	0.48 ± 0.02	50.2
1	1.25 ± 0.07	1.15 ± 0.03	1.1	0.049 ± 0.001	25.5
2	0.32 ±0.02	1.19 ± 0.06	−3.7	0.064 ± 0.0002	5.0
3	10.2 ± 0.13	34.1 ± 2.30	−3.3	0.17 ± 0.006	60.0
4	3.37 ± 0.17	3.91 ± 0.09	−1.2	1.19 ± 0.07	2.8
5	4.89 ± 0.17	4.39 ± 0.30	1.1	0.39 ± 0.03	12.5
6	9.81 ± 0.02	6.35 ± 0.67	1.5	2.00 ± 0.05	4.9
7	4.28 ± 0.34	4.81 ± 0.30	−1.1	2.94 ± 0.23	1.5
8	0.36 ± 0.03	4.51 ± 0.02	−12.5	0.20 ± 0.004	1.8
9	0.30 ± .005	20.5 ± 1.33	−68.3	0.69 ± 0.04	−2.3
10	0.37 ± 0.02	1.31 ± 0.07	−3.5	0.083 ± 0.003	4.5
11	1.21 ± 0.03	1.70 ± 0.07	−1.4	0.23 ± 0.02	5.3
12	2.59 ± 0.13	1.04 ± 0.07	2.5	0.43 ± 0.009	6.0
13	0.33 ± 0.003	0.49 ± 0.012	−1.5	0.097 ± 0.003	3.4
14	2.66 ± 0..27	1.10 ± 0.05	−2.4	1.03 ± 0.07	2.6
15	5.16 ± 0.20	7.52 ± 0.31	−1.5	1.83 ± 0.09	2.8
16	5.83 ± 0.47	9.20 ± 0.69	1.6	1.60 ± 0.12	3.6
17	11.7 ± 0.05	10.4 ± 0.75	1.1	1.64 ± 0.14	7.1

Table 3

Crystallographic Statistics

Crystallography Statistics	BaWT/2	BaWT/6	BaY102F/2	BaY102F/6	BaY102F/5	BaY102F/TMP	BaF96I/TMP
PDB Code	3JVX	3JWM	3JWC	3JWK	3JWF	3JW5	3JW3
Space Group	$P4_2$	$P4_2$	$P4_2$	$P4_2$	$P4_2$	$P4_2$	$P4_2$
No. Monomers in Asymmetric Unit	2	2	2	2	2	2	2
Unit cell (a,b,c in Å)	a,b=78.24 c=66.98	a,b=78.88 c=67.43	a,b=77.85 c=67.10	a,b=77.86 c=67.53	a,b=77.89 c=67.06	a,b=74.99 c=67.41	a,b=75.43 c=67.46
Resolution (Å)	28.59-2.25	38.95-2.57	42.56-2.57	42.68-2.08	38.95-2.57	37.50-2.89	41.85-2.57
Completeness % (last shell*, %)	99.9 (99.4)	98.8 (98.1)	99.7 (96.5)	100.0 (100.0)	98.7 (92.4)	98.2 (86.0)	99.7 (96.2)
Unique reflections	18,299	12,154	12,210	23,117	12,126	7,952	11,538
Redundancy (last shell)	6.6(6.5)	7.6(7.7)	7.0(4.7)	7.3(7.3)	5.4(3.4)	6.6(3.7)	7.0(4.7)
Rsym, % (last shell, %)	0.142 (0.512)	0.057 (0.154)	0.114 (0.391)	0.161 (0.463)	0.122 (0.232)	0.179 (0.443)	0.110 (0.407)
$\langle I/\sigma \rangle$ (last shell)	12.6(3.0)	41.9(14..9)	19.9(3.3)	26.1(4.9)	22.8(4.6)	11.6(2.3)	22.1(3.2)
R-factor/R_{free}	0.182/0.2098	0.198/0.243	0.191/0.230	0.183/0.213	0.208/0.257	0.212/0.261	0.219/0.262
Number of atoms (protein, ligands, solvent)	2805,49, 233	2766, 51, 193	2758,49, 116	2769,51, 361	2758,49, 118	2766,41, 37	2768,41, 37
Rms deviation bond lengths (Å), angles (°)	0.009, 1.323	0.008, 1.264	0.008, 1.296	0.010, 1.398	0.007, 1.185	0.008, 1.294	0.010, 1.371
Average B factor for protein ($Å^2$)	27.18	19.70	24.29	24.96	30.57	33.56	33.99
Average B factor for ligand ($Å^2$)	24.98	29.82	24.23	28.53	31.27	38.07	43.56
Average B factor for solvent molecules ($Å^2$)	34.01	22.17	22.75	33.31	28.17	20.71	28.189
Residues in most favored regions (%)	90.3	90.6	91.3	91.0	90.6	87.5	88.5
Residues in additional allowed regions (%)	9.7	9.4	8.7	9.0	9.4	12.5	11.5